ICAS-88-1.5R1

RAREFIED-FLOW PITCHING MOMENT COEFFICIENT MEASUREMENTS OF THE SHUTTLE ORBITER

R. C. Blanchard*
NASA Langley Research Center
Hampton, Virginia 23665-5225

and

E. W. Hinson**
ST Systems Corporation
28 Research Drive
Hampton, Virginia 23666

Abstract

An overview of the process for obtaining the Shuttle Orbiter rarefied-flow pitching moment from flight gyro data is presented. The extraction technique involves differentiation of the output of the pitch gyro after accounting for non-aerodynamic torques such as those produced by gravity gradient and the Orbiter's auxiliary power unit and adjusting for drift biases. The overview of the extraction technique includes examples of results from each of the steps involved in the process, using the STS-32 mission as a typical sample case. The total pitching moment and moment coefficient, C_m, for that flight are calculated and compared with preflight predictions. The flight results show the anticipated decrease in C_m with increasing altitude. However, the total moment coefficient is less than predicted using preflight estimates.

Nomenclature

A	Orbiter reference area (249.91 m^2, 2690 ft^2)
C_A	axial force coefficient
CG	center of gravity
C_m	pitching moment coefficient
C_{m_o}	basic pitching moment coefficient ($\alpha = 40°$, $\delta_E = \delta_{BF} = 0°$, baseline CG)
C_N	normal force coefficient
$\bar{C}$	Orbiter mean aerodynamic chord (12.06 m, 39.56 ft)
e_i	error coefficients for y-axis rate gyro calibration
GMT	Greenwich Mean Time
I_{xx}, I_{yy}, I_{zz}	moments of inertia about principal axes
I_{xz}	product of inertia, x-z axes
Kn	Knudsen number
k	constant relating $\Delta C_{m_{RG}}$ to Kn
M	pitching moment
M_{gg}	pitching moment induced by gravity gradient
p	roll rate
q	pitch rate
$\dot{q}$	angular acceleration about pitch axis
R	radius from center of Earth to Orbiter
r	yaw rate
t	time
v	velocity
x_i	variable or modeled terms in y-axis rate gyro calibration
α	pitch angle of attack
δ_{BF}	body flap deflection angle
δ_E	elevon deflection angle
δ_R	rudder deflection angle
$\Delta C_{m_{BF}}$	change in C_m due to flap
ΔC_{m_E}	change in C_m due to elevon
$\Delta C_{m_{RG}}$	correction to predicted C_m for real-gas effect
ΔC_{m_α}	change in C_m due to angle of attack
Δx	difference in x component between actual and baseline CG
Δz	difference in z component between actual and baseline CG
μ_E	Earth gravitational constant
ρ	atmospheric density

*Senior Research Engineer, Aerothermodynamics Branch, Space Systems Division.
**Chief Scientist.

Subcripts

I inboard

L left

O outboard

Introduction

Preflight estimates of aerodynamic characteristics for a complex delta wing vehicle like the Space Shuttle Orbiter are a combination of wind-tunnel tests and computation techniques in the hypersonic regime and mostly empirical extrapolations into the rarefied regime. During reentry, each Orbiter traverses all the flight regimes, ranging from free-molecular flow to subsonic continuum, and thus provides a means by which all flow regimes can be investigated. Instruments onboard the Orbiter are now providing actual flight data which can be used to examine the degree of conservatism used in preflight estimates. Quality onboard sensors have provided aerodynamic force data in the rarefied-flow regime during high altitude (low density) and high velocity conditions.[1]

During the first flights of the Shuttle Orbiter, a pitching moment discrepancy at high altitude in the hypersonic regime during reentry was discovered.[2] Early analyses of the flight data suggested a more forward center of pressure resulting in a trimmed body flap deflection angle of twice the predicted value. Initially, the moment differences were attributed to scaling, but subsequent studies isolated the differences to real-gas effects[3] which were treated as a tolerance in the initial data base formulations. For flight, real-gas flow processes generate smaller normal force coefficients than wind-tunnel measurements, and the center of pressure moves forward significantly, thus causing a more positive (nose up) pitching moment coefficient, C_m.

Earlier studies[4] of the Orbiter pitching moment were confined to altitudes below 95 km in the hypersonic portion of flight where the Orbiter is aerodynamically trimmed using control surfaces. Flight derived pitching moment coefficients from these studies were inferred from the behavior of the control system, i.e., from the body flap deflection attitude history. Above 95 km, the control surfaces are set at fixed positions, and attitude is controlled by impulsive thrusters. The fixed positions of the control surfaces, although not the same for each flight, aid the direct determination of pitching moment coefficient from onboard gyro data. This report summarizes the procedure and presents an overview of selected results of the pitching moment coefficient extracted from gyro data taken during Orbiter reentries.

Orbiter Geometry

Aerodynamic Sign Conventions

The adopted sign convention for the aerodynamic coefficients in this study is shown in Fig. 1. The convention used is the same as for conventional aircraft. The longitudinal pitching moment coefficient, C_m, is the principal coefficient under examination, and its reference center is the actual center of gravity of the vehicle.

Control Surfaces

Figure 2 is a sketch that identifies the control surfaces on the aft portion of the Shuttle Orbiter. These movable surfaces are the rudder/speed brake on the tail, the dual elevon surfaces on the trailing edge of each wing, and the body flap surface below the main engine nozzles on the bottom of the fuselage. The elevons provide longitudinal control as well as lateral trim and control when operated differentially as ailerons. The corresponding Orbiter vehicle aerodynamic control surface sign conventions are illustrated in Fig. 3. For instance, a positive body flap deflection angle, δ_{BF}, (body flap down) produces a negative moment coefficient (nose down). An effective δ_E is used which is an average of the inner and outer elevon surfaces. For the entire region investigated, the rudder/speed brake deflection angle $\delta_R = 0°$. Only two control surface angles are considered, namely δ_E and the body flap deflection angle, δ_{BF}.

Control Surface Deflections

Gauges are placed on each control surface mechanism to indicate relative position, i.e., deflection angles from nominal. Typical body flap angles (δ_{BF}) and elevon angles (δ_E) from an altitude of 160 km to 60 km for several Shuttle flights are given in Fig. 4. Note that the control surfaces do not become activated until the Shuttle has descended to approximately 95 km. Below this altitude, the vehicle transitions from spacecraft to aircraft, and the control surfaces are exercised in order to establish aerodynamic control. Of course, during this time, the control jets are still active. For the most part, only small angle-of-attack excursions are experienced. That is, angle of attack is held constant, close to 40°, with a small dispersion about this angle for each reentry.

Moment Extraction Technique

The net pitching moment acting on the Orbiter can be calculated from the relation

$$M = I_{yy}\dot{q} + (I_{xx} - I_{zz})pr - I_{xz}r^2 + I_{xz}p^2$$

Yaw and roll rates are small during the high altitude segment of Orbiter reentry, allowing the approximation

$$M = I_{yy}\dot{q}$$

where $\dot{q}$ is obtained from differentiation of the output of the pitch rate gyro. This section presents the moment extraction technique with examples shown for the STS-32 mission.

An experimental Aerodynamic Coefficient Instrument Package, ACIP, containing rate gyros was installed on the Orbiters Columbia, OV-102, and Challenger, OV-99. Data were recorded in flight for a period beginning before the deorbit burn maneuver and ending at landing. After flight, the tape recorder was downloaded, and the data were transformed to engineering units, then correlated with trajectory parameters, such as angle of attack and altitude.

Figure 5 shows the results of averaging the raw pitch rate gyro data over an interval around entry interface during the STS-32 mission. The Reaction Control System (RCS) thruster firings shift the pitch rate periodically to maintain the average inertial rotation rate (approximately -.067°/sec) necessary to hold the 40° pitch angle of attack during reentry. The drift periods between thruster firings clearly show the long term slope due to the net moment from aerodynamic forces, propulsive forces, and gravity gradient torque. Removing the discontinuities due to thruster firings produces the result shown in Fig. 6. This result can be viewed somewhat as the pitch rate history that would occur in the attitude drift mode from the initial rate with no thruster activity. In reality, the pitch rate in drift would diverge from that shown in Fig. 6 due to variation of aerodynamic moment as the angle of attack moved away from 40°. However, the pitching moment is proportional only to the slope of pitch rate, so differentiation of the q-time history in Fig. 6 produces the correct result. Figure 7 shows the variation of $\dot{q}$ obtained by differentiating the q-time history in Fig. 6. Further smoothing of the data was accomplished during this step by solving for the slope with a linear regression. Finally, Fig. 8 shows the net moment resulting from multiplying $\dot{q}$ by the appropriate value of I_{yy}.

The net moment must be considered to include gravity gradient torque and the Auxiliary Power Unit (APU) moment in order to isolate the moment due to aerodynamic forces only. The gravity gradient torque is calculated from the approximate relation

$$M_{gg} = \frac{3\mu_E}{R^3}\left(I_{xx} - I_{zz}\right) \sin\alpha \cos\alpha$$

where μ_E is the Earth gravitation constant, R is the vehicle distance from the center of the Earth, I_{xx} and I_{zz} are the principal inertia components, and α is the angle of attack. This torque is a maximum of ± 19 N-m (14 ft-lb) when the Orbiter is aligned with the x-body axis at an angle of 45° with the local vertical. At the reentry altitude, the value is about 16 N-m (12 ft-lb), which is considered to be negligible in this analysis. The APU torque is considerably larger, about 276 N-m (204 ft-lb).

The APU's are turned on in the following sequence. The first APU is turned on several minutes prior to the deorbit burn, and the second and third units are turned on together several minutes after the deorbit burn is completed. Estimates of the change in moment at these turn-on times were made for each flight and produced an average of 92 N-m (68 ft-lb) per APU or 276 N-m (204 ft-lb) for all three during reentry. Figure 9 shows a typical plot of the net moment around the turn-on time for the first APU.

The resolution of $\dot{q}$ obtained in this analysis depends on the q channel rate gyro resolution and the time interval over which the slope of q is determined. A moment of 54 N-m (40 ft-lb) will change q at a rate which represents the absolute limit of detectability for the pitching moment. Increasing the time interval over which the slope is determined improves the resolution, and this was done to obtain estimates of the APU torques.

Errors in the calculated moments are the result of errors in the rate gyro system which manifest themselves in the slope of q versus time. Examination was made of the equation in Ref. 5 for calculation of q from flight data. The equation has the form

$$q = \sum_i e_i x_i$$

where the coefficients e_i are determined during preflight calibration and the x_i are either modeling terms or flight-measured variables. This summation accounts for mechanical/electrical bias, scale factor, misalignment crossfeed, temperature bias and scale factor, and linear "g" sensitivity of the gyro (end effect). There are four terms which satisfy the conditions that x_i is time dependent and e_i is not zero. Three of these four terms produce worst case error corrections which imply moment correction less than the resolution of this analysis procedure. Since the correction itself is below the limit of detectability, errors in the correction terms would be even less significant. The fourth term involves the y-axis rate gyro scale factor, e_9, and the y-axis rate gyro output, x_9, whose product represents the uncorrected q; i.e., the above equation reduces to

$$q = e_9 x_9$$

when neglecting the error correction terms. Differentiating this equation with respect to time gives

$$\dot{q} = e_9 \frac{dx_9}{dt}$$

Consequently, shifts in the scale factor after calibration will cause a proportionate error in $\dot{q}$. No postflight recalibration was performed, and no means were provided for inflight verification of scale factor. A good first-order check can be made by using the APU moments as a standard. APU moments calculated from the actual data from the nine flights averaged 92 N-m (68 ft-lb) with a standard deviation of 5.3 N-m (3.9 ft-lb). This result was heavily biased by one flight (STS-8) which produced a moment of 88 N-m (65 ft-lb). Deleting this flight yields a standard deviation of only 2.6 N-m (2 ft-lb) or 3 percent of the mean. This clearly indicates that no significant shift in the scale factor has occurred over the nine flights.

The calculated aerodynamic moments above 130 km are very noisy with mean values ranging from 41 to 95 N-m (30 to 70 ft-lb). Investigation of the moments from this altitude up to orbital altitude shows a long period variation of about 68 N-m (50 ft-lb) modulating the total moment. The source of this oscillating bias has not been determined to date. It is compensated for by forcing the moment at 160 km (in free-molecular flow) to a value consistent with the Schaaf and Chambre model[6] employed in the Hypersonic Arbitrary Body Program which was used to calculate preflight free-molecule flow values for C_m.[7,8] That model yields a pitching moment coefficient of -0.31 for $\alpha = 40°$, $\delta_{BF} = \delta_E = 0°$. This procedure affects the flight-derived moments very little below 120 km but yields more realistic values in the range of 120 to 130 km.

Flight Results

Pitching Moments

Pitching moments from ACIP data were calculated by the described procedure with the result from STS-32 shown in Fig. 10 for the altitude range 95 to 130 km. The upper altitude limit is imposed by the measurement resolution of the instrument. The lower limit is the altitude at which the control surfaces become active during the transition from RCS to aerodynamic control. Variations in the magnitudes of the moments have been observed from flight to flight. These are due to different elevon and body flap deflection angles and to variations in the center-of-gravity (CG) location.

Curves showing the preflight "predicted" aerodynamic pitching moments are also included in Fig. 10. This moment was calculated from the relation

$$M = \frac{1}{2} \rho v^2 C_m A \bar{C}$$

where A and $\bar{C}$ are Orbiter reference values of 249.91 m^2 and 12.06 m (2690 ft^2 and 39.56 ft), respectively; v is the Orbiter velocity obtained from the postflight Best Estimated Trajectory (BET);[9] ρ is atmospheric density from the 1962 U.S. Standard Atmosphere;[10] and C_m is the pitching moment coefficient from the Orbiter Design Data Book adjusted for the as-flown values of α, δ_{BF}, δ_E, and CG location. The use of many flight-measured and postflight-determined parameters makes these moments "predicted" primarily because of the use of the preflight C_{m_o}, $\Delta C_{m_{BF}}$, and ΔC_{m_E}. In general, the preflight estimates consistently overpredict the magnitude of the moments. Examination of these differences requires calculation of the moment coefficient which is discussed next.

Pitching Moment Coefficient

The flight-extracted pitching moment coefficients obtained in this analysis were calculated from the above relation rearranged as follows

$$C_m = \frac{2M}{\rho v^2 A \bar{C}}$$

where ρ is derived from flight acceleration measurements.[11] The results of this calculation are shown on Fig. 11. Also shown on this figure are the preflight predictions for the pitching moment coefficient based on the Orbiter Design Data Book and the 1962 U.S. Standard Atmosphere. The preflight predictions are calculated from the relation

$$C_m = C_{m_o} + \Delta C_{m_{EL}} + \Delta C_{m_{BF}} + \Delta C_{m_\alpha} + \frac{\Delta x}{\bar{C}} C_N + \frac{\Delta z}{\bar{C}} C_A$$

where C_{m_o} is the basic pitching moment coefficient for baseline CG location, 40° angle of attack, and zero elevon and body flap deflection. The delta terms correct the basic coefficient to actual CG location, angle of attack, and control surface deflections as flown. The atmosphere model provides density at altitude for estimation of Knudsen number upon which the models for C_N and C_A are dependent.

As expected from the moment measurements, the flight-derived pitching moment coefficient is much smaller than predicted by the Orbiter Design Data Book. Part of the difference at lower altitudes is due to the well known real-gas effect,[12] based upon Maus's computational flowfield work and other analyses.[13] Real-gas effects were expected and were included in the uncertainties in the aerodynamics that the Orbiter was designed to handle with its flight control system. Figure 12, taken from Ref. 11, shows the flight-derived normal- and axial-force coefficients as a function of Knudsen number and also shows the comparison of wind-tunnel data, for which no correction for real-gas effect was made. The real-gas effect shows up only in C_N, which indicates that C_m is also affected. An approximate correction for the real-gas effect on C_m is of the form

$$\Delta C_{m_{RG}} = k (\log_{10} Kn - 1) \quad 10^{-3} \leq Kn \leq 10$$

where k is a constant based upon existing real-gas computations.[3] This model assumes that real-gas effects become progressively less with increasing Knudsen number and completely disappear in the free-molecule flow regime. The correction, as applied to the preflight predictions, is shown on Fig. 11 and indicates an improvement at low altitudes. It is also possible that the rarefied flow C_N is not modeled properly or that the pressure distribution over the Orbiter is not properly determined, or a combination of both.

Summary

A technique for obtaining the pitching moment in the rarefied-flow flight regime of the Shuttle Orbiter has been obtained. This has been applied to several reentry flights with some

success; an example of the technique as applied to STS-32 is presented as a demonstration. In terms of altitude, the regime investigated is in the rarefied transition regime, from hypersonic continuum into the free-molecule-flow region. It is anticipated that as altitude increases, Reynolds number decreases with an associated increase in viscous interaction effects. Simultaneously, as altitude increases, real-gas effects should diminish due to less enthalpy in the thickening boundary layer. These combined effects are contained in the flight data.

The procedure used to extract the pitching moment involves differentiation of the pitch rate gyro data after accounting for thruster effects and adjusting for other non-aerodynamic moments. The pitching moments compared with preflight estimates tend, in general, to be less, suggesting that Shuttle planners used conservatism in the construction of the original aerodynamic data base. The postflight pitching moment coefficient for STS-32 shows the classical decrease where viscous interaction effects are seen to create a more negative C_m as altitude increases. This, of course, corresponds to an aft shift in the center of pressure as expected. Correcting the preflight pitching moment coefficient for real-gas effects (estimated by Maus in the hypersonic continuum regime) tends to provide better agreement at lower altitude. However, differences remain at higher altitudes which are most likely attributable to errors in the empirical predictions methodology.

References

[1]Blanchard, R. C., "Rarefied Flow Lift-to-Drag Measurements of the Shuttle Orbiter," 15th Congress of International Council of Aeronautical Sciences (ICAS), Paper No. ICAS-86-2.10.2, September 1986.

[2]Romere, P. O., Kanipe, D. B., and Young J. C., "Space Shuttle Entry Aerodynamics Comparisons of Flight with Preflight Predictions," Journal of Spacecraft and Rockets, Vol. 20, January-February 1983, pp. 15-21.

[3]Maus, J. R., Griffith, B. J., Szema, K. Y., and Best, J. T., "Hypersonic Mach Number and Real-Gas Effects on Space Shuttle Orbiter Aerodynamics," Journal of Spacecraft and Rockets, Vol. 21, March-April 1984, pp. 136-141.

[4]Shuttle Performance: Lessons Learned, compiled by J. P. Arrington and J. J. Jones, Part I, Entry Aerodynamics I and II, NASA CP-2283, March 1983.

[5]Kinzger, M. J., "Aerodynamics Coefficient Identification Package (ACIP) Calibration Report, Calibration 2, January 1983," Lockheed Eng. and Management Services Co., Contract NAS9-15800, November, 1983. (Refer to JSC-19362).

[6]Schaaf, S. A. and Chambre, P. L., "Flow of Rarefied Gases," Fundamentals of Gas Dynamics, Howard W. Emmons, ed., Princeton Univ. Press, 1958, pp. 687-738.

[7]"Aerodynamics Design Substantiation Report - Vol. I: Orbiter Vehicle," Rockwell International, Space Division, SD74-SH-0206-1H, January 1975.

[8]Aerodynamics Design Data Book - Vol. I: Orbiter Vehicle, JSC-19654, April 1978.

[9]Compton, H. R., Findlay, J. T., Kelly, G. M., and Heck, N. L., "Shuttle (STS-1) Entry Trajectory Reconstruction," AIAA Paper No. 81-2459, November 1981.

[10]U. S. Standard Atmosphere, 1962, NASA, USAF, USWB, December 1962.

[11]Blanchard, R. C., Hinson, E. W., and Nicholson, J. Y., "Shuttle High Resolution Accelerometer Package Experiment Results: Atmospheric Density Measurements Between 60-160 km," AIAA Paper No. 88-0492, January 1988.

[12]Vancamberg, P., "Experimental and Theoretical Tests for Prediction of Aerodynamic Moments of HERMES in Hypersonic Flight," 15th Congress of International Council of Aeronautical Sciences (ICAS), Paper No. ICAS-86-2.10.1, September 1986.

[13]Woods, W. C., Arrington, J. P., and Hamilton, H. H. II, "A Review of Preflight Estimates of Real-Gas Effects on Space Shuttle Aerodynamic Characteristics," NASA CP 2283, March 1983.

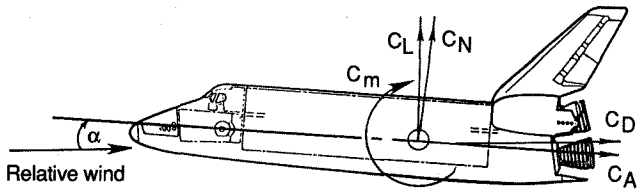

Fig. 1 Aerodynamic coefficient sign conventions.

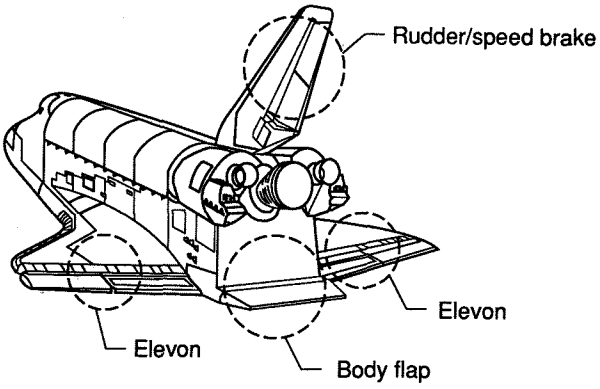

Fig. 2 Shuttle Orbiter aerodynamic control surfaces.

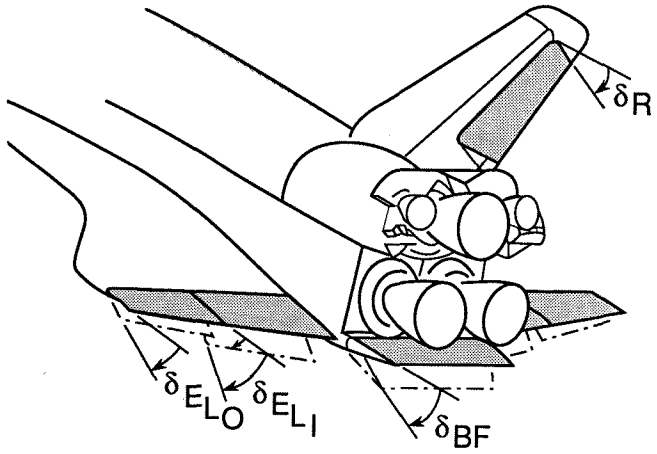

Fig. 3 Aerodynamic control surface sign conventions.

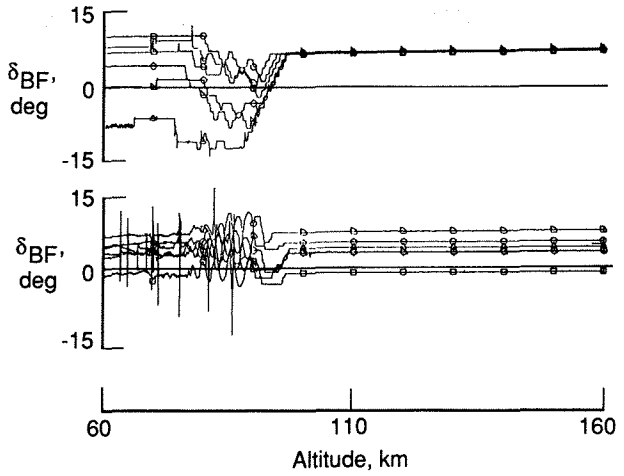

Fig. 4 Typical reentry control surface deflections.

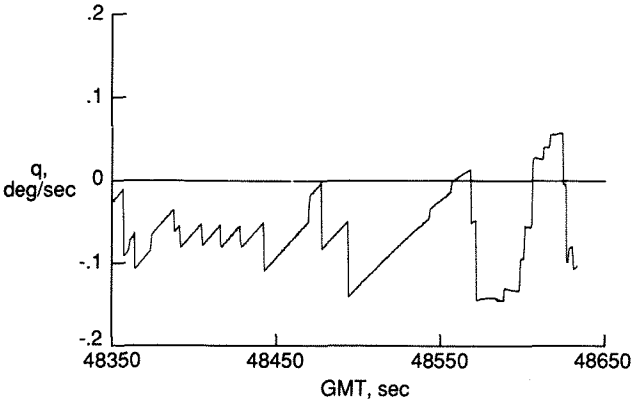

Fig. 5 Averaged angular velocity about y-axis, STS-32.

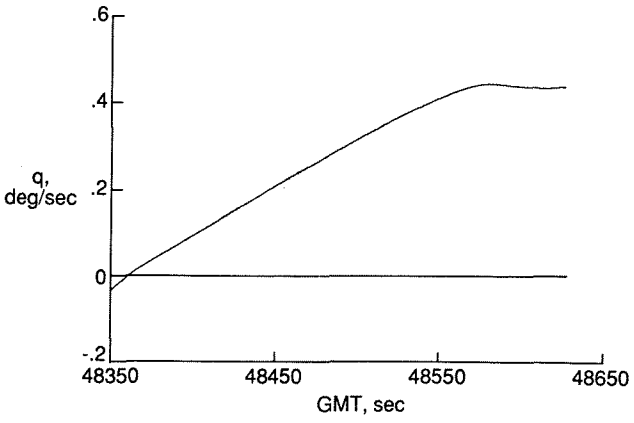

Fig. 6 Adjusted angular velocity about y-axis, STS-32.

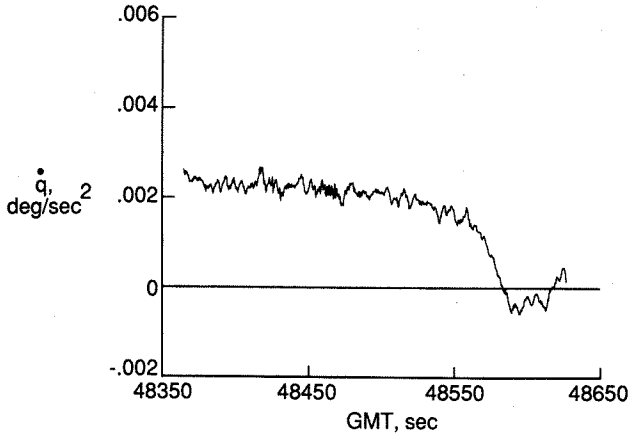

Fig. 7 Angular acceleration about y-axis, STS-32.

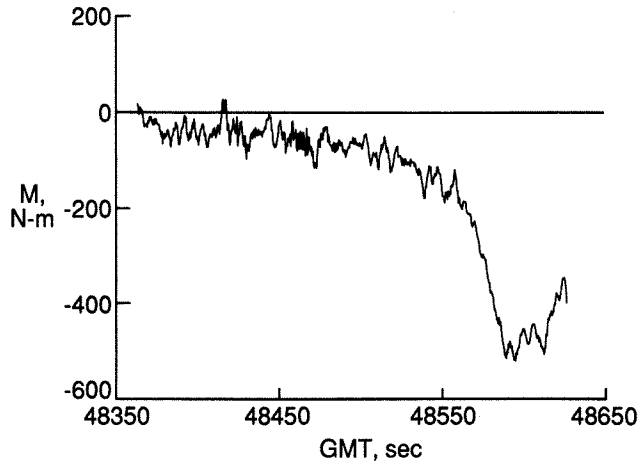

Fig. 8 Orbiter pitching moment, STS-32.

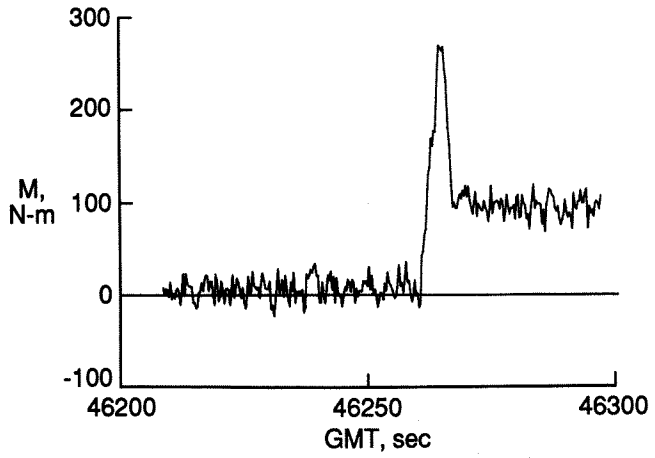

Fig. 9 Typical Orbiter pitching moment at APU start.

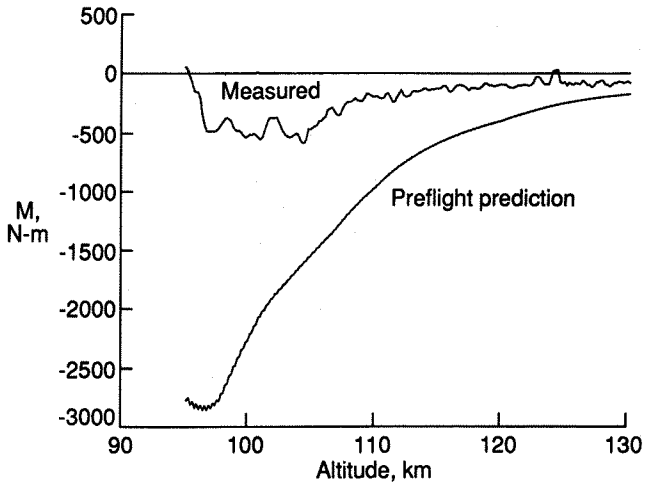

Fig. 10 Orbiter pitching moment, STS-32.

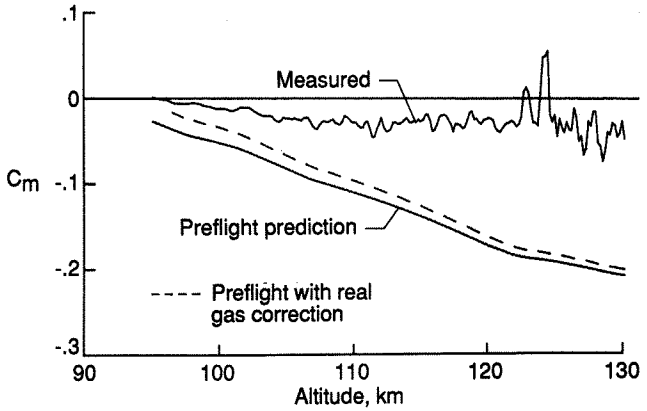

Fig. 11 Orbiter pitching moment coefficient, STS-32.

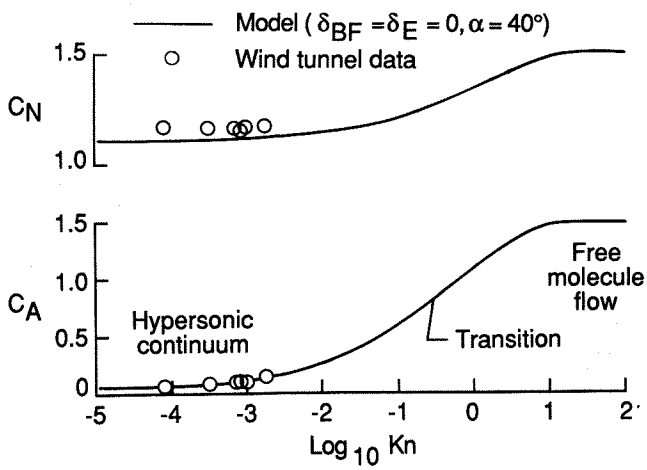

Fig. 12 Comparison of wind-tunnel data with normal and axial force coefficient analytic models derived from flight data.